Enhanced, robust light-driven H_2 generation by gallium-doped titania nanoparticles

Si Luo,[a,b] Thuy-Duong Nguyen-Phan,[a*†] Dimitriy Vovchok,[a,b] Iradwikanari Waluyo,[c] Robert Palomino,[a] Andrew D. Gamalski,[d] Laura Barrio,[e] Wenqian Xu,[f] Dmitry E. Polyansky,[a] José A. Rodriguez[a,b] and Sanjaya D. Senanayake[a] *

The splitting of water into molecular hydrogen with the use of sustainable solar energy has been considered as one of the most promising routes to yield sustainable fuel. Herein we report the H_2 evolution performance of gallium doped TiO_2 photocatalysts with varying degrees of Ga doping. The gallium ions induced significant changes in structural, textural and electronic properties of TiO_2 nanoparticles, resulting in remarkably enhanced photocatalytic activity and good stability for H_2 production. Ga species can act as the hole traps that efficiently facilitate the photoexcited electron transfer and thus charge separation. Additionally, the cationic dopant and induced defects might introduce the mid-gap state, promoting the electron migration and prolonging the lifetime of charge carrier pairs. We have discovered that the optimal Ga dopant concentration was 3.125 at% and then the incorporation of platinum (0.5 wt%) as a co-catalyst further improved the H_2 evolution rate up to 5722 μmol g^{-1} h^{-1} which can be ascribed to the intimate interaction between Pt and Ga-TiO_2 leading to improved interfacial electron transfer process. These catalyst design startegies provide new ways of designing transition metal photocatalysts that improve green H_2 fuel production from sustainable solar energy and water.

Introduction

Photocatalytic water splitting using semiconductor particles is one of the most promising routes to produce clean hydrogen fuel using renewable solar energy.[1-4] Despite enormously considerable progress has been made using highly active TiO_2 photocatalysts, it is still challenging to achieve efficient catalytic activity either by retarding the recombination of electron-hole pairs upon photoexcitation or to improve responsiveness to visible light absorption because of their large intrinsic band gap.[1-4] In most cases, it is necessary to load cocatalysts (*i.e.* Pt) onto the TiO_2 surface not only to enhance the electron mobility and transfer, thus increasing the separation of charge carriers, but also to provide active sites for redox reactions.[1-4]

Doping foreigner elements into the TiO_2 host is one of the most effective approaches to facilitate the charge carrier separation by altering its electronic structure, leading to better apparent quantum efficiency.[1-4] Cationic doping with transition metals, *i.e.* Cu, Fe, Ni, Ce, Al, Mn, Ga, Ru, etc., has been extensively reported to enhance the performance.[4-12] However, it is noteworthy that doping does not always introduce favourable effects, for instance, the defects induced by excess dopant might work as the recombination centers of photo-excited electrons and holes, thus diminishing the quantum efficiency. The fundamental understanding of doping effects in terms of structural changes is essential to take advantage of resulting phenomena and ascertain the optimal doping concentrations. For instance recently, Al-She'irey et al.[13] reported that Ga doping into the (001)-faceted TiO_2 microtablet significantly enhanced the interfacial interactions between TiO_2 and perovskite layer, and the carrier transport in the solar cell device, leading to 2.46% improved power conversion efficiency. In this work, we report the doping of earth abundant, less expensive, gallium species into TiO_2 nanoparticles with various gallium concentrations using a combined co-precipitation method. The influence of Ga dopants on the photocatalytic H_2 production from water with and without a Pt cocatalyst is systematically investigated. The correlation between the physico-chemical-electronic property alteration and superior UV-Vis light activity achieved by Ga doping is also discussed.

Experimental

Synthesis of Ga-doped TiO_2 nanoparticles

All the reagents are purchased from Sigma Aldrich and used without further purification. In a typical procedure, solution A including titanium (IV) isopropoxide (Ti-$(OC_3H_7)_4$) and 50 mL of isopropanol (IPA) was prepared at room temperature. Otherwise, a desirable amount of gallium (III) nitrate hydrate ($Ga(NO_3)_3.xH_2O$) was dissolved in 25 mL of IPA and 0.86 mL of deionized water (solution B). Solution B was sequentially added into solution B, following by slowly adding 4.8 mL of aqueous ammonia solution (NH_4OH, 28%) using a syringe pump (1 mL min^{-1}). The mixture was kept stirring at room temperature for 16 h, and evaporated at 80 °C until free dry powder was obtained. The as-synthesized product was subsequently calcined in ambient air at 500 °C for 2 h and denoted as 'xGaTi' where x is nominal Ga doping concentration, x = 1.56, 3.125, 6.25 and 12.5 at%. The undoped TiO_2 was prepared by same method without the usage of gallium precursor in solution B.

The loading of Pt co-catalyst (0.5 wt%) on Ga-doped TiO_2 was prepared for water splitting measurement by the wetness impregnation method. 8.5 mL of aqueous chloroplatinic acid solution ($H_2PtCl_6.6H_2O$, 0.3 mM) was slowly added to the mixture of 0.1 g xGaTi and 20 mL of deionized water at 85 °C

[a.] *Chemistry Department, Brookhaven National Laboratory, Upton, NY 11973, US*
[b.] *Department of Chemistry, Stony Brook University, Stony Brook, NY 11790, US*
[c.] *Photon Sciences Division, National Synchrotron Light Source II, Brookhaven National Laboratory, Upton, NY 11973, US*
[d.] *Center for Functional Nanomaterials, Brookhaven National Laboratory, Upton, NY 11973, US*
[e.] *CSIC - Instituto de Catalisis y Petroleoquimica Cantoblanco, E-28049 Madrid, Spain*
[f.] *X-ray Science Division, Advanced Photon Source, Argonne National Laboratory, Argonne, Illinois 60439, US*
† Current affiliation: National Energy Technology Laboratory, AECOM, Pittsburgh, PA 15236, US. Email: ThuyDuong.NguyenPhan@netl.doe.gov
Electronic Supplementary Information (ESI) available: Fig. S1-S3 include XRD patterns, time profiles of water splitting reaction, and performance comparison. See DOI: 10.1039/x0xx00000x

Please do not adjust margins

under vigorous stirring. After fully evaporated, the powder was dried for 2 h and annealed at 500 °C for 3 h. The Pt-impregnated sample was labelled as 'Pt/xGaTi'.

Characterizations

Synchrotron X-ray powder diffraction (XRD) patterns were collected at beamline 17-BM-B (λ = 0.72768 Å) of the Advanced Photon Source at Argonne National Laboratory. Powder samples were loaded into a 1.0 mm-diameter kapton capillary and two-dimensional diffraction patterns were collected by a Perkin Elmer amorphous silicon detector. The data acquisition was integrated by QXRD while the crystalline phase identification, composition and lattice parameters were subsequently analyzed by Rietveld refinement using GSAS-2 program.

X-ray absorption spectra (XAS) were obtained at beamline 23-ID-2 (CSX-2) of the National Source Light Source II at Brookhaven National Laboratory (BNL). Powder samples were mounted on an Al foil and loaded into the analysis chamber. The XAS measurements are collected using total electron yield (TEY) detection mode to provide sensitive chemical state information relevant to the Ga L-edge, Ti L-edge and O K-edge.

The Brunauer-Emmett-Teller (BET) specific surface area and total pore volume were determined by N_2 sorption measurement conducted on a Micromeritics ASAP2020 apparatus at −196 °C. The samples were degassed at 150 °C for 6 h prior to analysis.

Other characterization techniques were performed at the Center for Functional Nanomaterials at BNL. High angle annular dark field scanning transmission electron microscopy (HAADF-STEM) images were collected on a Hitachi HD2700C at accelerating voltage of 200 kV. Electron energy loss spectroscopy (EELS) mapping was recorded by Bruker Nano GmbH detector. X-ray photoelectron spectroscopy (XPS) was recorded on a RHK-XPS/STM/AFM system using Mg Kα source and a hemispherical analyser (PHOIBOS HSA-3500 100). The survey spectra were collected with a pass energy of 50 eV whereas the core-level spectra were measured with a pass energy of 20 eV. All the binding energies were calibrated to the surface adventitious hydrocarbon feature (C 1s) at 284.6 eV. Raman spectra were collected on a WiTec Alpha combination microscope with 532 nm laser as an excitation source. UV-Vis diffuse reflectance (UV-Vis-DRS) measurements were performed on PerkinElmer Lambda 950 spectrometer equipped with an integrating sphere assembly.

Photocatalytic water splitting measurement

The photocatalytic water splitting activity was evaluated through the measurement of hydrogen evolution (half-reaction) in a closed gas circulation and evacuation system. 3 mg of powder catalyst were suspended in 3 mL of aqueous methanol solution (20 vol%) in a 6-mL sealed quartz cell. The reaction temperature was maintained at 293 K by continuous water circulation. After evacuation and Ar purging several times to remove the dissolved oxygen in the solution ensuring the anaerobic condition, the reactor was side-irradiated by a 150 W Xenon arc lamp from Optical Building Blocks Corporation equipped with a $CuSO_4$ filter (310 nm < λ < 625 nm) under magnetic stirring. The evolved gases were determined by gas chromatography (GC Agilent 6890N) equipped with FID/TCD detectors and methanizer using Ar as the carrier gas.

Results and Discussion

Figure 1A shows a HAADF-STEM micrograph of 3.125 at%Ga-doped TiO_2 nanoparticle in which the mean particle size is in range of 6-10 nm. The doped TiO_2 nanoparticles are well-defined crystallized and their smooth surface without the contrast difference implies the absence of free access or unbound gallium related species. A well-resolved lattice fringe of 0.35 nm corresponds to the (101) plane of anatase TiO_2. No obvious contraction or expansion of *d*-spacing upon doping was found by electron microscopy. The effective ionic radius of Ti(IV) is 60.5 pm in the six coordination site of anatase structure whereas those for Ga(III) are 47 and 62 pm in 4- and 6-coordinate, respectively.[14] However, the Pauling ionic radii of Ti^{4+} and Ga^{3+} are 68 and 62 pm.[15] Such a comparable ionic radius may be favourable for the substitutional doping of Ga ions into TiO_2 matrix. Among five crystalline modifications of gallium oxide (α, β, γ, δ, and ε),

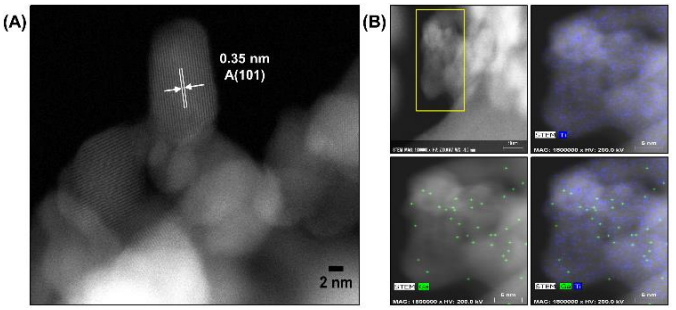

Fig. 1 (A) HAADF-STEM image and (B) EELS elemental maps of Ti (blue) and Ga (green) of 3.125Ga-doped TiO_2.

monoclinic β-Ga_2O_3 is the most stable crystalline form in which Ga ions are in distorted tetrahedral (corner sharing) and octahedral sites (edge sharing).[16-19] β-Ga_2O_3 could be obtained from other forms of Ga_2O_3 by annealing above 1000 °C[16] or from heat treatment of gallium nitrate at > 650 °C.[19,20] Considering the post treatment at 500 °C in air herein, the possible crystal phases are δ- and ε-Ga_2O_3, which were reported to present under lower temperature calcination.[16,20] δ-Ga_2O_3 is body-centered cubic metastable structure while ε-Ga_2O_3 is orthorhombic with obvious lower symmetry than hexagonal or tetragonal.[16,20,21] Herein, no fingerprint of any of five crystalline modifications of gallium oxide was observed in the STEM images. The EELS elemental maps in Figure 1B display the homogeneous distribution of Ga and Ti where the scarcity of Ga was recorded besides the enrichment of Ti signals.

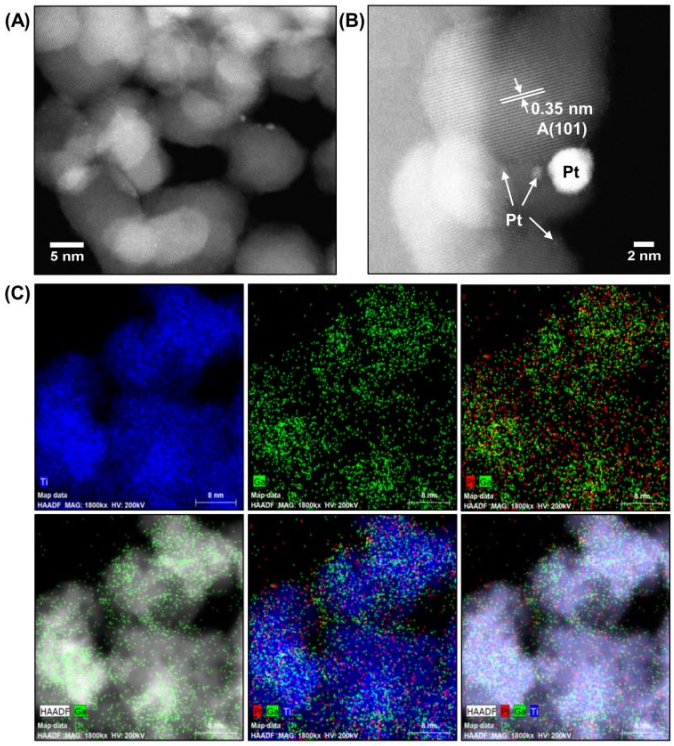

Fig. 2 (A, B) HAADF-STEM images; and (C) EELS elemental mapping of Ga (green), Pt (red), and Ti (blue) of 0.5Pt/3.125Ga-doped TiO_2.

Figure 2A-B shows representative HAADF-STEM images of Pt loaded on 3.125 at% Ga-doped TiO_2 nanoparticle. The contrast difference obviously indicates the existence of small Pt nanoparticles dispersed on the surface or surrounding doped TiO_2. The particle size of Pt varies from 0.5 to 4 nm. With more detailed mapping at different sites in Figure 2C, the gallium signals were well dispersed through the whole region of TiO_2 and no separated surface Ga species was found. Compared to Pt signals that were evenly distributed onto TiO_2 surface, the Ga signal was stronger in the thicker, agglomerated areas with more concentrated Ti. Therefore, Ga was believed to locate inside the lattice of TiO_2 framework, at least partially, meanwhile either the amorphous phase or ultra-small gallium oxide clusters on the surface could not be ruled out by electron microscopy.

In order to identify the crystal structure and lattice fringes compared with electron microscopic images, synchrotron XRD measurements were conducted. Figure 3A shows the XRD patterns of Ga-doped TiO_2 prepared at different Ga doping concentrations. It is clear that the diffraction peaks at 2θ = 11.9, 17.6, 22.2, 24.8, 25.2 and 28.5° for all samples match well with TiO_2 anatase phase ($I4_1/amd$ space group). It is in good agreement with the microscopic results. Very small fraction of rutile is detected at 12.9° in pure TiO_2. No noticeable diffraction peak representative of gallium species, *i.e.* cubic δ-Ga_2O_3 and γ-Ga_2O_3, monoclinic β-Ga_2O_3, or orthorhombic ε-Ga_2O_3, appears which can be attributed to the entire substitution of Ga ions into TiO_2 framework, very low concentration of gallium dopant and/or highly dispersed ultra-small gallium oxide clusters. As mentioned earlier, the comparable ionic radii between Ga^{3+} and Ti^{4+} might result in the substitution of Ga ion into lattice TiO_2 along with the interstitial doping sites. Chandiran et al.[7] suggested the trivalent Ga cation to be positioned as a substituent of Ti^{4+} site entailing the formation of oxygen vacancies at 2% Ga doping. It is worth noting that (101), (004), (200), (105) and (211) peaks are less intense along with slightly wider peak width with increasing Ga doping to 6.25 at%, indicating a decrease in the crystallite size. It is noted that the XRD peak shift and broadening can be attributed to the particle size-broadening effect and/or strain-broadening effect.[22] As seen in Table 1, the lattice parameters of anatase TiO_2 from Rietveld refinement slightly reduce in the presence of Ga up to 6.25 at% and then increase in 12GaTi sample. It is consistent with small shifts of the enlarged (101) peaks (shown in the inset) toward higher 2θ on 3.125GaTi, 6.25GaTi and 12.5GaTi. Accordingly, the average crystallite size decreases from 14.1 to 7.8 nm and become larger in Ga-rich sample (9.1 nm). Indeed, the crystallite size decreasing can be attributed to the doping effect that was

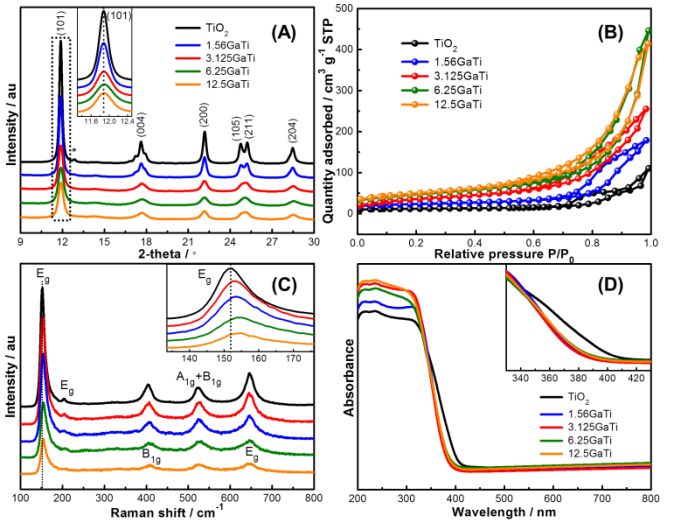

Fig. 3 (A) XRD patterns (* represents rutile phase, inset is enlarged (101) diffractions; (B) N_2 sorption isotherms; (C) Raman spectra (inset is enlarged view of E_g mode); and (D) UV-Vis-DRS spectra (inset is the zoom-in region of 330-430 nm) of TiO_2 and xGaTi series.

Table 1. BET surface area and Rietveld refinement of undoped and Ga-doped TiO_2 series.

Samples	BET surface area / m^2g^{-1}	Pore volume / cm^3g^{-1}	Lattice constant a / Å	Lattice constant c / Å	Average particle size / nm
TiO_2	45	0.17	-	-	-
1.56GaTi	86	0.28	3.785(8)	9.481(0)	14.1
3.125GaTi	133	0.39	3.785(0)	9.458(9)	9.4
6.25GaTi	168	0.69	3.783(6)	9.444(8)	7.8
12.5GaTi	176	0.64	3.784(6)	9.457(0)	9.1

widely reported in metal-doped TiO_2 systems.[6,7] Otherwise, the lattice constant *c* was found to decrease with increasing Ga concentrations from 1.56 to 6.25 at% as a consequence of the surface tension. Such a lattice shrinkage here could be caused by Ga^{3+} substitution with relatively smaller radius replacing Ti^{4+}, resulting in the distortion and contraction of lattice constant. As

the Ga dosage was further increased to 12.5 at%, such a substitutional doping was saturated and more free, ultra-small amorphous gallium oxide clusters tend to form on the TiO2 surface that could not be detected by XRD. No change is observed in the crystal structure of doped TiO_2 after Pt deposition as shown in XRD patterns in Figure S1 (ESI).

The reduction in crystallite size seems to be in good agreement with the gradual increase in BET surface area summarized in Table 1. The adsorption/desorption isotherms in Figure 3B are of type IV, characteristic of mesoporous materials according to IUPAC classification.[23] The isotherms have a well-defined hysteresis loop in the intermediate shape among type H2, H3 and H4 due to capillary condensation associated with aggregated particles having micropore filling. Doping gallium results in the better mesoporosity involving larger surface area (86 ~ 176 $m^2\ g^{-1}$) and total pore volume (0.28 ~ 0.69 $cm^3\ g^{-1}$) in comparison with undoped TiO_2 (45 $m^2\ g^{-1}$). The largest surface area for 12.5GaTi (~ 176 $m^2\ g^{-1}$) can be due to the formation of free ultra-small Ga_2O_3 nanoparticles that are aggregated on TiO_2 surface.[6,11]

Raman spectra of all samples in Figure 3C reveal five Raman-active modes at 152, 204, 646 (E_g), 405 (B_{1g}), and 523 cm^{-1} (A_{1g}+B_{1g}) which are indicative of anatase phase, hence corroborating STEM and XRD results. No molecular vibration for Ga-related species is tracked, *i.e.* 15 active modes for β-Ga_2O_3.[17] However, the most intense mode, E_g, which is associated to O-Ti-O bending vibration, blue-shifts from 152 to 155 cm^{-1} with increasing Ga dopant concentration (see in the inset). The shifting towards higher frequency can be caused by the shorter bond length of O-Ti bonding due to gallium incorporation that is in good agreement with diffraction results. It is also reported that the blueshift in phonon frequencies is due to the size confinement effect whereas the presence of impurities and defects causes the redshift.[17] So, combined with XRD data, such a small blueshift herein might be ascribed to the strain effect upon doping.

Figure 3D shows the UV-Vis-DRS spectra of blank TiO_2 and doped materials. The absorption edge of undoped TiO_2 locates at ~ 400 nm, corresponding to the band gap energy of 3.15 eV. Gallium doping strongly blue-shifts the onset toward lower wavelength regime meanwhile the absorption in range of 200-380 nm representative of O 2*p* (valence band) - Ti 3*d* (conduction band) hybridization obviously enhances compared to TiO_2. It demonstrates the less pronounced localization of 3*d* states or weaker hybridization between Ti 3*d* and Ga 3*d* in the presence of Ga ions and therefore wider 3*d* bands. Similar phenomena were reported in Chandiran et al and Al-She'irey et al.'s works,[7,13] where the light absorption is less upon Ga doping. Gionco et al.[10] theoretically and experimentally found that the substitution of a six-coordinated Ti atoms in anatase TiO_2 with Ga atoms induces the formation of a hole from TiO_2 VB which is strongly localized on the O 2*p* nonbonding orbital of a three-coordinated O atom. Such a superhyperfine interaction leads to a singly occupied α state at the VB maximum (VBM) and in an empty β component in the middle of the gap.[10] By time dependent density functional theory, Rahane et al.[24] reported the strong dependency of calculated optical absorption spectra and corresponding optical band gap for bulk stoichiometry $(Ga_2O_3)_n$ clusters on cluster geometries and size. With increasing cluster size, the absorption peaks shifted toward the higher energy range and such a blue shift may be the outcome of the bulk-like coordination.

The electronic structures of doped TiO_2 were also identified by XPS analysis and Auger spectroscopy. The high-resolution core-level spectra of Ti 2p in Figure 4A confirm the presence of Ti^{4+} states in terms of spin-orbital splitting of Ti $2p_{3/2}$ and Ti $2p_{1/2}$ at 459.5 and 456.2 eV, respective. Neither binding energy shift in Ti 2p doublets nor emerging shoulder for lower oxidation state of titanium species was detected upon Ga doping or Pt addition. Nevertheless, we found very small difference from O 1s feature. As seen in Figure 4B, O 1s spectra are asymmetric, involving the main peak at 530.8 eV representative of lattice oxygen and the shoulder at higher biding energy (+1 ~ +1.5 eV) which is usually attributed to oxygen vacancy defect, surface low-coordinated oxygen ion, surface hydroxyl group and/or surface adsorbed-molecular water. It could be noticed that Ga doping results in more pronounced shoulder compared to pure

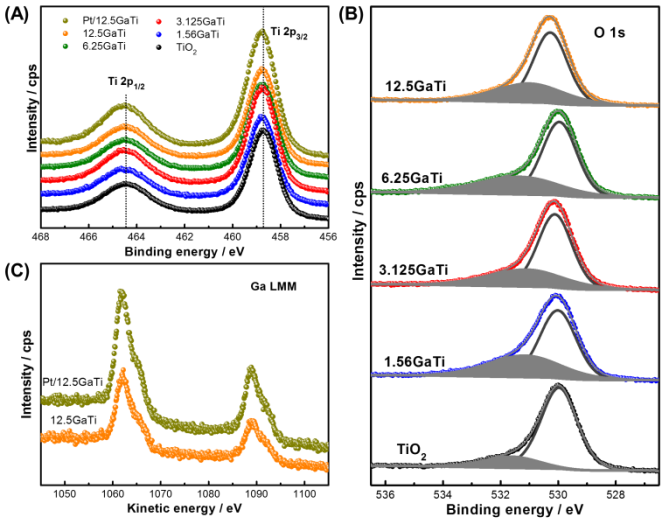

Fig. 4 (A) Ti 2p and (B) O 1s core-level XPS spectra of undoped and doped TiO_2; (C) Ga LMM Auger spectra of 12.5GaTi and Pt/12.5GaTi.

TiO_2, implicating the possible formation of more defects or under-coordinated oxygen species. The Ga LMM Auger spectra of 12GaTi with and without Pt in Figure 4C are consistent with the Ga LMM from Ga_2O_3 in literature with the predominant feature at ~1062 eV, while the reduced Ga species should display a peak at higher kinetic energy (for instance, metallic Ga at ~1069 eV). The Ga species, indeed, is mainly in a trivalent state although minor intermediate GaO_x might exist as the feature could be hidden in the Ga(III) LMM spectra.[25]

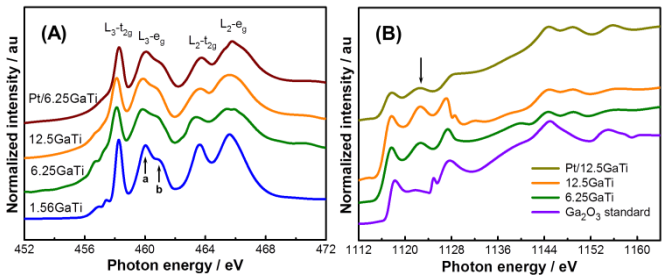

Fig. 5 (A) Ti L-edge and (B) Ga L-edge XAS spectra of Ga-doped TiO_2 samples.

X-ray absorption spectroscopy was employed to further characterize the electronic structure of Ga doped TiO_2 series. The Ti $L_{2,3}$-edge of 1.56GaTi sample in Figure 5A shows a classic, strong and sharp feature in range of 455-470 eV of anatase Ti(IV)O_2 which is assigned to excitations of the Ti 2p states into the empty Ti 3d states.[26,27] L_3-edge ($2p_{3/2}$ levels) and L_2-edge ($2p_{1/2}$ level) splits into two sub-bands associated with t_{2g} and e_g states via hybridization. The asymmetry of the L3-eg doublet is the fingerprint of the crystallographic phases that is ascribed to a noncubic ligand field effect related to the distortion of [TiO_6] octahedral environment.[28,29] Two weak, low-intensity pre-peaks arising from particle-hole coupling in an octahedral crystal field[28,29] are found. As the gallium concentration increases to 12.5%, the line shape remains similar to pure anatase TiO_2, indicating no obvious phase transformation. Nevertheless, with increasing Ga concentration, two pre-peaks disappear, the L_2-edge becomes broadening, and the L_3-e_g peak shows a noticeable flattering trend. The relative intensity ratio of (a/b) peaks in a symmetric L_3-e_g doublet decreases, reflecting the changes in long-range bonding (band structure) properties or electronic structure on a length scale of 1 nm due to Ga incorporation into the anatase lattice.[28,29] The broadening of L_2-edge originates from the shorter lifetime of 2p1/2 state[29] or from the band formation and/or much weaker excitonic effect for the more strongly hybridized e_g orbitals.[28] It should be noted that the addition of Pt herein does not alter the electronic structure of Ga-doped TiO_2 sample.

Figure 5B displays the Ga L-edge of bulk Ga_2O_3 reference, Ga-doped TiO_2 with 6.25 and 12.5% Ga, and Pt loaded samples. No signals of Ga were detected on low doping dosage materials (not shown here). The main distinguishable peak positions of doped TiO_2 are alike Ga_2O_3 standard, confirming trivalent oxidation state of tetrahedral gallium. It is noteworthy that the small features in the 1115 ~ 1130 eV region are very different from reference. Since Ga_2O_3 has various crystal modifications, the comprehensive interpretation of Ga L-edge respect to different crystal structure is devoid in literature. Shimizu et al.[21,30] compared the Ga L_3-edge spectra of various Ga_2O_3 materials and claimed that the second feature (marked by arrow) arising from 2p → 4d transition was related to low coordinated Ga with specific local structure. It is well consistent with our previous hypothesis that the amount of Ga incorporation into anatase TiO_2 lattice is limited. As Ga concentration increment beyond 6.25 at%, the Ga species would disperse on the surface of TiO_2 nanoparticles in form of ultra-small clusters with low coordination.

The photocatalytic H_2 production using Ga-doped TiO_2 photocatalysts without Pt cocatalyst is displayed in Figure 6A in which those materials demonstrate they are active for H_2 evolution. The time profiles in Figure S2A (ESI) show that a constant amount of H_2 is generated during 5 h of UV-visible light exposure (λ = 310-625 nm). Doping with Ga significantly improve the photocatalytic performance of TiO_2 and 3.125 at% Ga doping is the optimal concentration, producing ~ 360 μmol g^{-1} of H_2 per hour. Beyond this doping amount, the rate gradually diminishes to 285 and 41 μmol g^{-1} h^{-1}, leading to much worse performance than that over pure TiO_2 in spite of much larger surface area. It has been reported previously that excess doping concentration leads to reduced activity due to (i) the coverage of free oxide aggregates that might hinder the light absorption, penetration and photoactivation, and (ii) the formation of recombination centers that might trap more electrons, neutralize the holes and thus increasing the recombination opportunity.[1-5,7-9,11,12] Moreover, gallium ions can play the role of hole traps that efficiently facilitate the electron transfer and charge separation, hence improving the photocatalytic activity. Ga dopants and induced defects possibly introduce the mid-gap state, resulting in better charge transport, particularly electron migration, and longer lifetime of electron/hole pairs. Chandiran et al.[7] experimentally claimed that Ga^{3+} prolonged the electron lifetime, enhanced the charge carrier collection efficiency, but did not influence the energy distribution of the trap states below the CB or induce an upward shift of CB edge. Gionco et al.[10] proved that the Ga dopant ions stabilize the hole trapping centers and as a consequence, the generation of electron-hole pairs under illumination results in the preferential formation of localized polaronic holes near the dopant, reducing the mobility of these charge carriers.

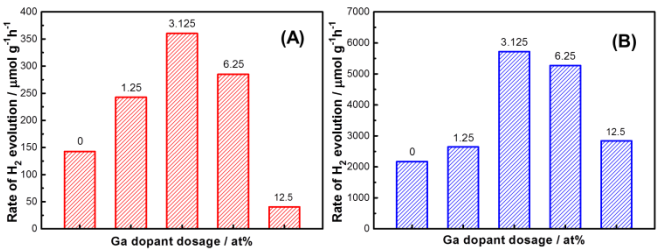

Fig. 6 Mass specific rate of H_2 evolution over undoped and Ga-doped TiO_2 (A) without and (B) with 0.5 wt% Pt co-catalyst under UV-Vis irradiation (λ = 310-625 nm).

With deposition of 0.5 wt% noble metal co-catalyst, the activity is significantly increased. Figure 6B shows the dependence of H_2 evolution rate on the Ga doping dosage in which the rate of H_2 production reaches a maximum, ~ 5722 μmol g^{-1} h^{-1}, at 3.125 at% of gallium dopant. Similar to non-co-catalyst case, excess doping content is detrimental to the photoactivity which is consistent with literature.[1-5,6,8,9] The remarkable enhancement in H_2 evolution rate in the presence of Pt nanoparticles, typically 10-15 times higher, can be explained by the effective trapping of excited electron from CB of doped TiO_2 system to Pt, thereby quenching the recombination of excited electrons and holes. It

is well known that Pt nanoparticles not only inhibits the quick backward reaction between O_2 and H_2 but also provides the active sites for the photocatalytic reaction. Joo et al.[31] experimentally demonstrated the alternative function of Pt to facilitate the recombination of atomic hydrogen that was not observed on carbon-TiO_2 catalysts.

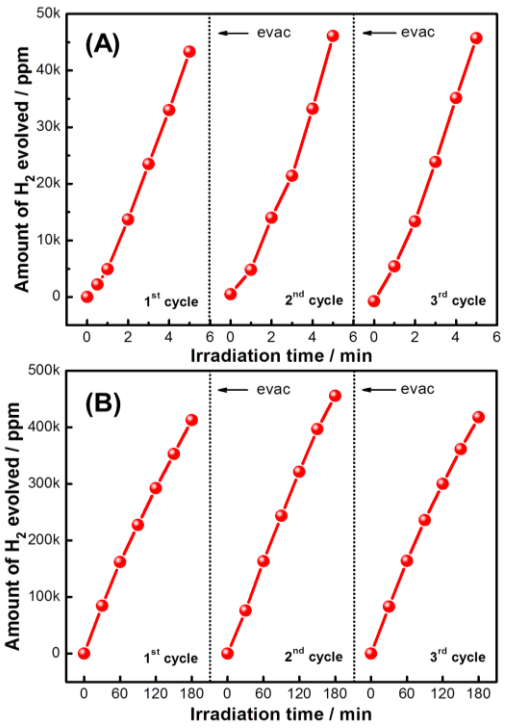

Fig. 7 Photocatalytic stability of H_2 generation over of 3.125% Ga-doped TiO_2 (A) without and (B) with Pt co-catalyst (λ = 310-625 nm, T = 298 K).

On the other hand, the durability is another crucial factor to evaluate a photocatalyst besides the catalytic activity since the deactivation or photo-corrosion easily occurs after few hours of light irradiation. To further probe the stability of these materials, two best photocatalysts, 3.125GaTi and Pt/3.125GaTi, were purged with Ar after a single run, evacuated overnight and re-measured the activity under light irradiation without photocatalysts washing or addition of fresh solution. As indicated in Figure 7, the amount of H_2 generation over both materials were quite stable after three consecutive cycles with each cycle of 5 h, implying the robustness of our photocatalysts.

Conclusions

Highly efficient Ga-doped TiO_2 photocatalysts with various gallium doping concentration was successfully developed. The optimal Ga doping dosage was 3.125 at%, and the addition of Pt co-catalyst remarkably improved H_2 evolution, producing 5722 μmol of H_2 per gram of catalyst per hour. The presence of gallium dopant exhibited significant photocatalytic activity and excellent durability for H_2 production due to the role as hole traps of Ga species that improve the electron transfer and charge separation. Moreover, the mid-gap state of cationic dopant and induced defects might be formed, leading to better electron transport and longer lifetime of electron/hole pairs. It is highly anticipated that our findings may provide design principles for promising transition metal photocatalysts for green H_2 fuel production from sustainable solar energy and water.

Acknowledgements

The research was performed at Brookhaven National Laboratory, supported by the U.S. Department of Energy, Office of Science, Office of Basic Energy Sciences, and Catalysis Science Program under contract No. DE-SC0012704. This work used resources of the Center for Functional Nanomaterials and National Synchrotron Light Source II at Brookhaven National Laboratory (Contract No. DE-SC0012704) and Advanced Photon Science at Argonne National Laboratory (Contract No. DE-AC02-06CH11357) which are DOE Office of Science User Facilities. Dr. Chinh Nguyen Huy (School of Chemical Engineering, University of Ulsan, South Korea) is acknowledged for N_2 sorption measurement.

References

1 A. Kudo and Y. Miseki, Heterogeneous Photocatalyst Materials for Water Splitting, *Chem. Soc. Rev.*, 2009, **38**, 253-278.

2 A. Kubacka, M. Fernández-García and G. Colón, Advanced Nanoarchitectures for Solar Photocatalytic Applications, *Chem. Rev.*, 2012, **112**, 1555-1614

3 Y.-P. Yuan, L.-W. Ruan, J. Barber, S. C. J. Loo and C. Xue, Hetero-Nanostructured Suspended Photocatalysts for Solar-To-Fuel Conversion, *Energy Environ. Sci.*, 2014, **7**, 3934-3951.

4 X. Zhou, N. Liu and P. Schmuki, Photocatalysis with TiO_2 Nanotubes - "Colorful" Reactivity and Designing Site-Specific Photocatalytic Centers into TiO_2 Nanotubes, *ACS Catal.*, 2017, **7**, 3210-3235.

5 N. Serpone, Is the Band Gap of Pristine TiO_2 Narrowed by Anion- and Cation-Doping of Titanium Dioxide in Second-Generation Photocatalysts?, *J. Phys. Chem. B*, 2006, **110**, 24287-24293.

6 V. Houšková, V. Štengl, S. Bakardjieva, N. Murafa and V. Tyrpekl, Efficient Gas Phase Photodecomposition of Acetone by Ru-Doped Titania, *Appl. Catal. B Environ.*, 2009, **89**, 613-619.

7 A. K. Chandiran, F. Sauvage, L. Etgar and M. Graetzel, Ga^{3+} and Y^{3+} Cationic Substitution in Mesoporous TiO_2 Photoanodes for Photovoltaic Applications, *J. Phys. Chem. C*, 2011, **115**, 9232-9240.

8 B. Liu, H. M. Chen, C. Liu, S. C. Andrews, C. Hahn and P. Yang, Large-Scale Synthesis of Transition-Metal-Doped TiO_2 Nanowires with Controllable Overpotential, *J. Am. Chem. Soc.*, 2013, **135**, 9995-9998.

9 Pérez-Larios, A. Hernández-Gordillo, G. Morales-Mendoza, L. Lartundo-Rojas, Á. Mantilla and R. Gómez, Enhancing the H_2 Evolution from Water-Methanol Solution using Mn^{2+}-Mn^{+3}-Mn^{4+} Redox Species of Mn-Doped TiO_2 Sol-Gel Photocatalysts, *Catal. Today*, 2015, **266**, 9-16.

10 C. Gionco, S. Livraghi, S. Maurelli, E. Giamello, S. Tosoni, C. Di Valentin and G. Pacchioni, Al- and Ga-Doped TiO_2, ZrO_2, and HfO_2: The Nature of O 2p Trapped Holes from a Combined Electron Paramagnetic Resonance (EPR) and Density Functional Theory (DFT) Study, *Chem. Mater.*, 2015, **27**, 3936-3945.

11 T.-D. Nguyen-Phan, S. Luo, D. Vovchok, J. Llorca, S. Sallis, S. Kattel, W. Xu, L. F. J. Piper, D. E. Polyansky, S. D. Senanayake, D. J. Stacchiola and J. A. Rodriguez, Three-Dimensional Ruthenium-Doped TiO_2 Sea Urchins for Enhanced Visible-Light-Responsive H_2 Production, *Phys. Chem. Chem. Phys.*, 2016, **18**, 15972-15979.

12 F. Gonell, A.V. Puga, B. Julián-López, H. García and A. Corma, Copper-Doped Titania Photocatalysts for Simultaneous Reduction of CO_2 and Production of H_2 from Aqueous Sulphide, *Appl. Catal. B Environ.*, 2016, **180**, 263-270.

13 A. Y. A. Al-She'irey, S. K. Md Saad, A. A. Umar, M. Y. A. Rahman and M. M. Salleh, (001) Faceted-Ga-TiO_2 Microtablet Synthesis and its Organic Perovskite Sensitized Solar Cells Characterization, *J. Alloys Comp.*, 2016, **674**, 470-476.

14 R. D. Shannon, Revised Effective Ionic Radii and Systematic Studies of Interatomic Distances in Halides and Chalcogenides, *Acta Crystallogr., Sect. A*, 1976, **32**, 751- 767.

15 B. W. Pfennig, *Principles of Inorganic Chemistry*, John Wiley & Sons, Inc., Hoboken, New Jersey, 2015.

16 R. Roy, V. G. Hill and E. F. Osborn, Polymorphism of Ga_2O_3 and the System Ga_2O_3-H_2O, *J. Am. Chem. Soc.*, 1952, **74**, 719-722.

17 R. Rao, A. M. Rao, B. Xu, J. Dong, S. Sharma and M. K. Sunkara, Blueshifted Raman Scattering and Its Correlation with the [110] Growth Direction in Gallium Oxide Nanowires, *J. Appl. Phys.*, 2005, **98**, 094312.

18 V. M. Bermudez, The Structure of Low-Index Surfaces of β-Ga_2O_3, *Chem. Phys.*, 2006, **323**, 193-203.

19 H. Y. Playford, A. C. Hannon, M. G. Tucker, D. M. Dawson, S. E. Ashbrook, R. J. Kastiban, J. Sloan and R. I. Walton, Characterization of Structural Disorder in γ-Ga_2O_3, *J. Phys. Chem. C*, 2014, **118**, 16188-16198.

20 K. Nishi, K. Shimizu, M. Takamatsu, H. Yoshida, A. Satsuma, T. Tanaka, S. Yoshida and T. Hattori, Deconvolution Analysis of Ga K-Edge XANES for Quantification of Gallium Coordinations in Oxide Environments, *J. Phys. Chem. B*, 1998, **102**, 10190-10195.

21 K. Shimizu, M. Takamatsu, K. Nishi, H. Yoshida, A. Satsuma, T. Tanaka, S. Yoshida and T. Hattori, Alumina-Supported Gallium Oxide Catalysts for NO Selective Reduction: Influence of the Local Structure of Surface Gallium Oxide Species on the Catalytic Activity, *J. Phys. Chem. B*, 1999, **103**, 1542-1549.

22 B. D. Cullity, *Elements of X-ray Diffraction*, Addison-Wesley Publishing Company, Inc., Reading, Massachusetts, USA, 1978.

23 M. Thommes, K. Kaneko, A. V. Neimark, J. P. Olivier, F. Rodriguez-Reinoso, J. Rouquerol and K. S. W. Sing, Physisorption of Gases, with Special Reference to the Evaluation of Surface Area and Pore Size Distribution (IUPC Technical Report), *Pure Appl. Chem.*, 2015, **87**, 1051-1069.

24 A. B. Rahane, M. D. Deshpande and S. Chakraborty, Optical Properties of Gallium Oxide Clusters from First-Principles Calculations, *J. Phys. Chem. A*, 2012, **116**, 10559-10565.

25 D. P. Butt, Y. Park and T. N. Taylor, Thermal Vaporization and Deposition of Gallium Oxide in Hydrogen, *J. Nucl. Mater.*, 1999, **264**, 71-77.

26 U. Diebold, The Surface Science of Titanium Dioxide, *Surf. Sci. Rep.*, 2003, **48**, 53-229.

27 P. Guttmann, C. Bittencourt, S. Rehbein, P. Umek, X. Ke, G. Van Tendeloo, C. P. Ewels and G. Schneider, Nanoscale Spectroscopy with Polarized X-rays by NEXAFS-TXM, *Nat. Photonics*, 2012, **6**, 25-29.

28 P. Krüger, Multichannel Multiple Scattering Calculation of $L_{2,3}$-Edge Spectra of TiO_2 and $SrTiO_3$: Importance of Multiplet Coupling and Band Structure, *Phys. Rev. B*, 2010, **81**, 125121.

29 F. M. F. De Groot, J. C. Fuggle, B. T. Thole and G. A. Sawatzky, $L_{2,3}$ X-ray-Absorption Edges of d^0 Compounds: K^+, Ca^{2+}, Sc^{3+} and Ti^{4+} in O_h (Octahedral) Symmetry, *Phys. Rev. B*, 1990, **41**, 928-937.

30 K. Shimizu, M. Takamatsu, K. Nishi, H. Yoshida, A. Satsuma and T. Hattori, Influence of Local Structure on the Catalytic Activity of Gallium Oxide for the Selective Reduction of NO by CH_4, *Chem. Commun.*, 1996, 1827-1828.

31 J. B. Joo, R. Dillon, I. Lee, Y. D. Yin, C. J. Bardeen and F. Zaera, Promotion of Atomic Hydrogen Recombination as an Alternative to Electron Trapping for the Role of Metals in the Photocatalytic Production of H_2, *Proc. Natl. Acad. Sci. U.S.A.*, 2014, **111**, 7942-7947.